Origin of magnetic anisotropy in the spin ladder compound $(C_5H_{12}N)_2CuBr_4$

D. Blosser [1,*] V. K. Bhartiya [1] D. J. Voneshen [2] and A. Zheludev [1,†]

[1]*Laboratory for Solid State Physics, ETH Zürich, 8093 Zürich, Switzerland*
[2]*ISIS Facility, Rutherford Appleton Laboratory, Chilton, Didcot, Oxon OX11 0QX, United Kingdom*

The $S = 1/2$ spin ladder compound $(C_5H_{12}N)_2CuBr_4$ (BPCB) is studied by means of high-resolution inelastic neutron scattering. In agreement with previous studies we find a band of triplet excitations with a spin gap of ∼0.8 meV and a bandwidth of ∼0.6 meV. In addition, we observe a distinct splitting of the triplet band of 50(1) μeV or 40(2) μeV at the band minimum or maximum, respectively. By comparison to a strong-coupling expansion calculation of the triplet dispersion for a spin ladder with anisotropic exchange, weakly anisotropic leg interactions are identified as the dominant source of magnetic anisotropy in BPCB. Based on these results, we discuss the nature of magnetic exchange anisotropy in BPCB and in related transition-metal insulators.

I. INTRODUCTION

The Heisenberg model is arguably the most important construct in quantum magnetism. Experimentally, it is usually studied in transition metal oxides and metal-organic salts. Unfortunately, symmetry-breaking magnetic anisotropy is unavoidable in such compounds. Even when weak compared to the dominant Heisenberg exchange, it can have a significant influence on the magnetic and dynamical properties. In understanding these, existing microscopic theories are usually disregarded in favor of minimalistic empirical models. For example, magnetic exchange interactions in insulators are described within Anderson's theory of superexchange [1–3]. In the presence of weak spin-orbit coupling it predicts both symmetric (Ising) and antisymmetric (Dzyaloshinskii-Moriya [DM]) exchange anisotropy always occurring in combination and at a fixed ratio [4–6]. Yet, experimental data are often successfully analyzed in comparison to a Heisenberg model with only an added DM term [7–11] even though such a model lacks microscopic justification. Even more often, signatures of weak magnetic anisotropy are detected in experiments, but their origin remains unknown altogether [12–14]. In short, anisotropy is ubiquitously present, yet pinpointing its microscopic origin is almost never possible.

Here we present a detailed case study: the effect of very weak magnetic anisotropy on spin excitations in the almost ideal Heisenberg quantum spin ladder compound $(C_5H_{12}N)_2CuBr_4$ (BPCB) [15–21]. On this compound we have obtained exceptionally high-resolution inelastic neutron-scattering data showing a small but distinct anisotropy splitting of the triplet excitations as described in Sec. II. At the same time, BPCB is an excellent realization of a strong rung spin ladder. It is described by only two exchange couplings: the rung exchange and an almost four times smaller

leg coupling. For this model, the excitation spectrum in the presence of various possible exchange anisotropies can be precisely calculated as detailed in Sec. III. This combination of high-resolution spectroscopic data and precise calculations of the excitation spectrum allows a detailed discussion of the anisotropy's microscopic origins in BPCB (Sec. IV). These findings we compare to the microscopic theory of anisotropic superexchange and we discuss how the present case study may guide our understanding of magnetic anisotropy in related compounds.

II. EXPERIMENT AND RESULTS

A. The compound $(C_5H_{12}N)_2CuBr_4$: Crystal structure and magnetic interaction pathways

The compound $(C_5H_{12}N)_2CuBr_4$, bis-piperidinium copper bromide or BPCB for short crystallizes in a monoclinic crystal structure with space group $P2_1/c$ and room-temperature lattice parameters $a = 8.49$, $b = 17.22$, $c = 12.38$ Å, and $\beta = 99.3°$ [15]. The spin ladders are formed by the magnetic Cu^{2+} cations carrying a spin $S = 1/2$ linked by superexchange bridges via Br^- anions [16]. The ladders run along the crystallographic a axis and are well separated by nonmagnetic organic piperidinium ions as depicted in Fig. 1 [22].

There are two crystallographically equivalent spin ladders in BPCB, related by the glide plane symmetry of the $P2_1/c$ space group. Furthermore, the center of each ladder rung corresponds to a crystallographic center of inversion symmetry. For this reason, on the ladder rungs, only symmetric exchange is possible [23], while for the ladder legs there are no symmetry restrictions and both symmetric and antisymmetric exchange are in principle allowed. On the ladder leg, the antisymmetric exchange contribution is parametrized by a Dzyaloshinskii-Moriya vector **D**. These DM vectors are uniform within every ladder leg and antialigned between the two legs of each ladder. The DM vectors of the two crystallographically equivalent ladders are again related by the reflection of the glide plane symmetry as sketched in
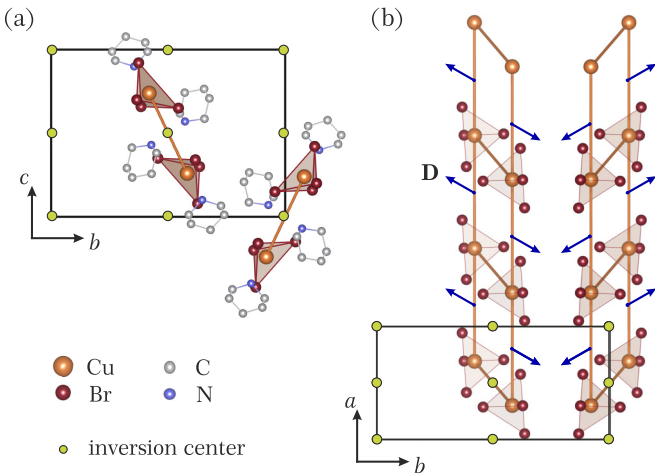
*dblosser@phys.ethz.ch
†zhelud@ethz.ch; http://www.neutron.ethz.ch/

144406-1

(a)

(b)

FIG. 1. Schematic of the crystal structure of BPCB. The spin ladders are formed by the magnetic Cu^{2+} cations and linking Br^- anions. Crystallographic centers of inversion symmetry are marked by green dots. Anisotropic Dzyaloshinskii-Moriya interactions, by symmetry, are only allowed on the ladder legs and possible DM vectors **D** are sketched as blue arrows on these bonds. Note that for this monoclinic structure, in both plots the third axis (projection axis) is not perpendicular to the plane of the figure.

Fig. 1. Besides these relations, the DM vectors may point in any direction and are not further constrained by symmetry. Similarly, The g tensors for the magnetic moments residing on the different Cu^{2+} ions show different principal axes for the two types of ladders. Thus, in an applied magnetic field, the two types of ladders become inequivalent, except for special orientations of the magnetic field [19,20]. In the present study, however, we exclusively focus on zero-field properties where the two ladders remain equivalent.

B. Inelastic neutron scattering

Neutron-scattering experiments were performed on four fully deuterated single crystals of total mass 2.07 g, co-aligned to better than 1° effective mosaic spread. The

FIG. 3. Cuts through the data shown in Fig. 2 at the band extrema: (a) Cut at the band minimum $q_{\parallel}/2\pi = -0.5$ through the 1.35-meV data set. (b),(c) Cuts at the band extrema $q_{\parallel}/2\pi = -0.5$ or $q_{\parallel}/2\pi = 0$, respectively, through the 2.20-meV data set. Solid lines correspond to Gaussian fits. At the band minimum we find a slightly larger splitting of $\Delta_{\min} = 50(1)$ μeV than at the band maximum where $\Delta_{\max} = 40(2)$ μeV.

measurements were carried out at the LET cold neutron time-of-flight spectrometer [24] at the ISIS facility, UK. The sample was mounted on a ^{3}He-^{4}He dilution refrigerator with the crystallographic b axis vertical. Making use of repetition rate multiplication, data were collected simultaneously using neutrons of incident energies $E_i = 1.35$, 2.20, 4.20, and 11.0 meV. For these configurations we find an approximately Gaussian energy resolution of 19, 36, 97, and 410 μeV at full width at half maximum, respectively, for elastic scattering ($\hbar\omega = 0$) and improving towards higher energy transfer.

C. Experimental results

An overview of the neutron-scattering data [25] collected for $E_i = 2.2$ and 1.35 meV at a temperature of 0.35 K is presented as false color intensity plots in Fig. 2. For this quasi-one-dimensional spin ladder system, the measured
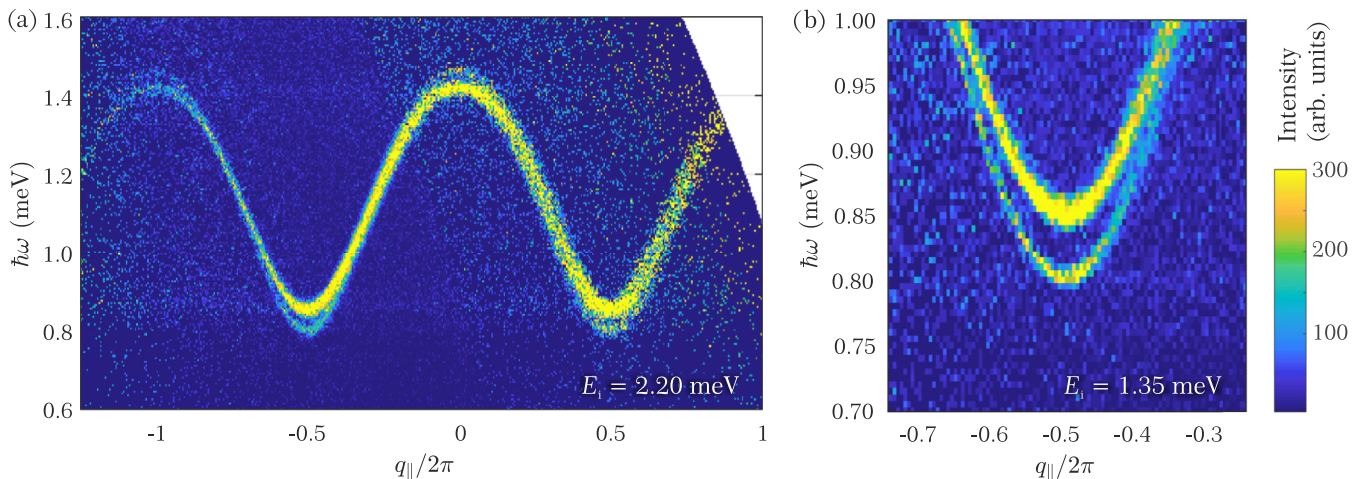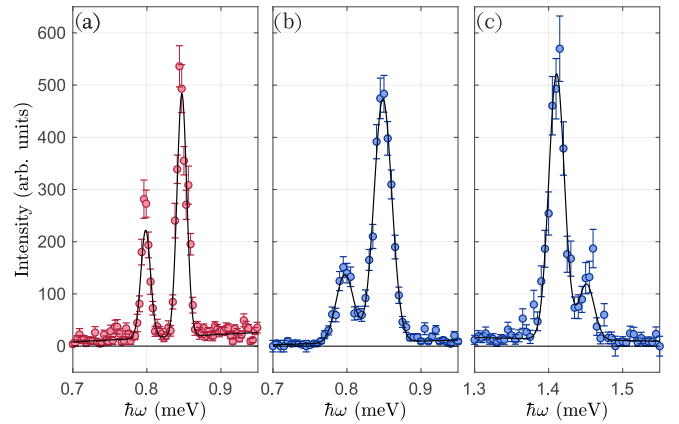

FIG. 2. False-color maps of the inelastic neutron-scattering intensity measured using (a) $E_i = 2.20$ meV and (b) $E_i = 1.35$ meV incident energy neutrons at $T = 0.35$ K. With the lower incident energy, a superior energy resolution is achieved but only the low-energy parts of the dispersion can be probed.

scattering intensity is plotted versus reduced wave-vector transfer parallel to the ladder $q_\parallel = \mathbf{Q} \cdot \mathbf{a}$ and integrated fully along the nondispersive b^* and c^* directions.

We observe a band of excitations with an excitation gap of $\Delta \sim 0.8$ meV and a bandwidth of $\Gamma \sim 0.6$ meV. The linewidth of gapped excitations in one-dimensional (1D) systems is known to show activation behavior [26]. With $k_B T \ll \Delta$, in the present experiment these excitations are long lived and their apparent width corresponds to the experimental resolution.

Cuts through both data sets at the band extrema are shown in Fig. 3. These correspond to the data of Fig. 2 integrated in thin slices of $q_\parallel/2\pi = -0.5 \pm 0.02$ and $q_\parallel/2\pi = 0 \pm 0.03$, respectively (the dispersion is less curved at the maximum allowing to integrate a wider slice for improved counting statistics). To these cuts we fit two Gaussian peaks of equal width and a linear background shown as a solid lines in Fig. 3. We find a splitting of $\Delta_{\min} = 50(1)$ μeV at the band minimum and $\Delta_{\max} = 40(2)$ μeV at the band maximum.

III. TRIPLET DISPERSION FOR A SPIN LADDER WITH EXCHANGE ANISOTROPY

A. Isotropic Heisenberg ladder

For an isotropic spin $S = 1/2$ ladder we denote the rung and leg Heisenberg exchange constants as $J_\perp$ and $J_\parallel$, respectively. In the limit of $\lambda = J_\parallel/J_\perp \ll 1$, the spin ladder can be understood as a 1D array of weakly interacting spin dimers. For $\lambda = 0$ the ground state corresponds to a product state of singlets and the low-energy excitations are triplet excitations. In the presence of weak leg coupling, these excitations become mobile and for small λ their dispersion can be calculated in a strong-coupling expansion [27]. For an isotropic ladder with Hamiltonian

$$\mathcal{H} = J_\perp(\mathcal{H}^\perp + \lambda \mathcal{H}^\parallel), \quad \mathcal{H}^\perp = \sum_{R=1}^{L} \mathbf{S}_{R,1} \cdot \mathbf{S}_{R,2}, \quad \mathcal{H}^\parallel = \sum_{R=1}^{L} \sum_{\alpha=1}^{2} \mathbf{S}_{R,\alpha} \cdot \mathbf{S}_{R+1,\alpha}, \tag{1}$$

up to third order in λ, the following dispersion is obtained in Ref. [27], degenerate for the three $\sigma = \{+, 0, -\}$ triplet branches:

$$\epsilon_\sigma(k)/J_\perp = 1 + \gamma \cos(k) + \frac{\gamma^2}{4}[3 - \cos(2k)] + \frac{\gamma^3}{8}[3 - 2\cos(k) - 2\cos(2k) + \cos(3k)]. \tag{2}$$

In the following we do the same calculation for a ladder with anisotropic rung or leg exchange, respectively. Some details of these computations are given in the Appendix.

B. Anisotropic rung interactions

In addition to the isotropic rung and leg couplings, here Ising-type anisotropy on the ladder rungs is considered. We choose the z axis parallel the Ising axis and consider the Hamiltonian

$$\mathcal{H} = J_\perp(\mathcal{H}^\perp + \lambda \mathcal{H}'), \quad \mathcal{H}' = \mathcal{H}^\parallel + C\,\mathcal{H}^{\mathrm{Rung,Ising}}, \quad \mathcal{H}^{\mathrm{Rung,Ising}} = \sum_{R=1}^{L} S_{R,1}^z S_{R,2}^z, \tag{3}$$

where the Ising anisotropy on the ladder rungs is parametrized by C. Using the same strong-coupling expansion as applied to the isotropic case in Ref. [27], up to third order in λ we find

$$\epsilon_0(k)/J_\perp = 1 + \lambda \cos(k) + \frac{\lambda^2}{4}[3 - \cos(2k)] + \frac{\lambda^3}{8}[3 - 2C - 2\cos(k) - 2\cos(2k) + \cos(3k)], \tag{4}$$

$$\epsilon_\pm(k)/J_\perp = 1 + \lambda\left[\frac{C}{2} + \cos(k)\right] + \frac{\lambda^2}{4}[3 - \cos(2k)] + \frac{\lambda^3}{8}[3 - 2C - 2\cos(k) + (C-2)\cos(2k) + \cos(3k)]. \tag{5}$$

C. Anisotropic leg interactions

Finally, we consider anisotropic exchange on the ladder legs with both symmetric and antisymmetric contributions. Assuming a center of inversion symmetry on the ladder rungs, we consider a uniform DM vector $+\mathbf{D}$ on one leg and $-\mathbf{D}$ on the other leg. Furthermore we include Ising anisotropy of independent magnitude but pointing in the same direction as $\mathbf{D}$. We choose the z axis parallel to $\mathbf{D}$ and consider

$$\mathcal{H} = J_\perp(\mathcal{H}^\perp + \lambda \mathcal{H}'), \quad \mathcal{H}' = \mathcal{H}^\parallel + B\,\mathcal{H}^{\mathrm{Leg,DM}} + A\,\mathcal{H}^{\mathrm{Leg,Ising}}, \tag{6}$$

$$\mathcal{H}^{\mathrm{Leg,DM}} = \sum_{R=1}^{L} \sum_{\alpha=1}^{2} (-1)^\alpha \mathbf{e}_z \cdot (\mathbf{S}_{R,\alpha} \times \mathbf{S}_{R+1,\alpha}), \quad \mathcal{H}^{\mathrm{Leg,Ising}} = \sum_{R=1}^{L} \sum_{\alpha=1}^{2} S_{R,\alpha}^z S_{R+1,\alpha}^z. \tag{7}$$

Up to third order in λ we find the following triplet dispersion:

$$\epsilon_0(k)/J_\perp = 1 + \lambda(1+A)\cos(k) + \frac{\lambda^2}{4}\left[3 - 4B^2 + 2A + A^2 + 4B^2\cos(k) - \left(1 + 2A + A^2\right)\cos(2k)\right]$$

$$+ \frac{\lambda^3}{8}\left[3 + 3A - \left(2 + 4B^2 + 4A + 4AB^2 + 3A^2 + A^3\right)\cos(k) - \left(2 + 2A - 4B^2 - 4AB^2\right)\cos(2k)\right.$$

$$\left. + \left(1 + 3A + 3A^2 + A^3\right)\cos(3k)\right], \tag{8}$$

$$\epsilon_\pm(k)/J_\perp = 1 + \lambda\cos(k) + \frac{\lambda^2}{4}\left[3 - 2B^2 + 2A + A^2 - \cos(2k)\right]$$

$$+ \frac{\lambda^3}{8}\left[3 + 3A - \left(2 + 12B^2 + A + \frac{A^2}{2}\right)\cos(k) - \left(2 + 2B^2 + 2A + 2AB^2\right)\cos(2k) + \frac{1}{8}\cos(3k)\right]. \tag{9}$$

IV. DISCUSSION

A. Discussion of experimental results

The experimental data shown in Fig. 2 closely resemble previously published results on BPCB with dispersive triplet excitations [16,19]. In these experiments the resolution was not sufficient to detect the small band splitting and those data were very well described using a model of an isotropic spin ladder with $J_\perp/k_B = 12.7(1)$ K and $J_\parallel/k_B = 3.54(3)$ K [21]. Only with the superior resolution of the present experiment is the small splitting of the triplet band observed.

In our data, perpendicular to the one-dimensional ladders, no dispersion is observed within the experimental resolution. This validates BPCB as an exceptionally one-dimensional ladder compound and it corroborates that the observed band splitting is inherent to the spin ladders and is not related to residual 3D interactions. In addition, interladder interactions were previously estimated on the order of a few 10s of mK [18] (a few μeV)—much smaller than the observed band splitting.

A previous ESR study on BPCB [20] found clear signatures of magnetic anisotropy, of exactly the same magnitude as the band splitting observed in the present experiments. By a careful study of the angular dependence of the ESR signal, an anisotropy axis tilted approximately $50°$ from the b axis in the $(b, c^\star)$ plane could be identified as a special direction. However, the origin of this anisotropy remained unclear.

One source of magnetic anisotropy is dipolar interactions present in all materials [28]. For classical magnetic moments at the shortest Cu-Cu distance found in BPCB, dipolar interactions are estimated as $J_{dipolar}/k_B \approx 6$ mK (< 1 μeV), much smaller than the observed band splitting. Dipolar interactions clearly can be ruled out as the primary cause of magnetic anisotropy in BPCB. Since for the $S = 1/2$ Cu^{2+} ions there cannot be any single-ion anisotropy, *exchange anisotropy* must be the dominant cause of the observed small splitting of the triplet band. Before further analyzing our data in this regard, we first discuss the nature of anisotropic superexchange interactions in the following section.

B. Anisotropic superexchange

Most generally, the effective exchange interaction between two spins takes the form $\mathcal{H}_{1,2} = \mathbf{S}_1 \Gamma \mathbf{S}_2$ where Γ is a tensor. Decomposing Γ into its symmetric and antisymmetric parts

and choosing a basis such that the symmetric part is diagonal, this can be written as

$$\mathcal{H}_{1,2} = J\,\mathbf{S}_1 \cdot \mathbf{S}_2 + \mathbf{D} \cdot (\mathbf{S}_1 \times \mathbf{S}_2) + \sum_{\alpha=x,y,z} G^\alpha\, S_1^\alpha S_2^\alpha. \tag{10}$$

Here, J is the isotropic (Heisenberg) exchange. The so-called Dzyaloshinskii-Moriya vector $\mathbf{D}$ quantifies the antisymmetric exchange and G^α ($\alpha = x, y, z$) determine the symmetric (Ising) exchange anisotropy where $\sum_\alpha G^\alpha = 0$.

Including spin-orbit coupling (SOC) into Anderson's theory of superexchange [1] indeed all these contributions are obtained [2,3]. However, in this setting, symmetric and antisymmetric interactions are not independent and, for a single bond, to a good approximation the superexchange interaction Hamiltonian reads [4–6]

$$\mathcal{H}_{1,2} = \left(J - \frac{|\mathbf{D}|^2}{4J}\right)\mathbf{S}_1 \cdot \mathbf{S}_2$$

$$+ \mathbf{D} \cdot (\mathbf{S}_1 \times \mathbf{S}_2) + \frac{1}{2J}(\mathbf{D} \cdot \mathbf{S}_1)(\mathbf{D} \cdot \mathbf{S}_2). \tag{11}$$

Here a *single* vector $\mathbf{D}$ defines both the symmetric and antisymmetric exchange. This expression, although not obvious, is fully invariant under spin rotations [5,6]: While the term $\mathbf{D} \cdot (\mathbf{S}_1 \times \mathbf{S}_2)$ acts to confine the spins to a plane perpendicular to the vector $\mathbf{D}$, the Ising contribution acts to align the spins with $\mathbf{D}$. Thus, for a single bond, anisotropic superexchange will never single out a particular direction. Nonetheless, for multiple connected bonds, *frustration* of the $\mathbf{D}$ vectors may still break spin rotation symmetry and lead to the appearance of anisotropy [5,6].

Besides this mechanism, considering multiple orbitals of the ligands transmitting the superexchange interactions in the presence of SOC may result in *additional* sources of exchange anisotropy, beyond Eq. (11). However, these additional effects have been argued to be much smaller in magnitude [29,30].

This leaves us with the following situation: When considering superexchange interactions, to first approximation symmetric and antisymmetric anisotropy contributions always come together pointing in the same direction and at a fixed ratio. In this case, if the center of a bond corresponds to a center of inversion symmetry, not only is antisymmetric exchange anisotropy forbidden by symmetry as is commonly known [23], but we also expect symmetric exchange
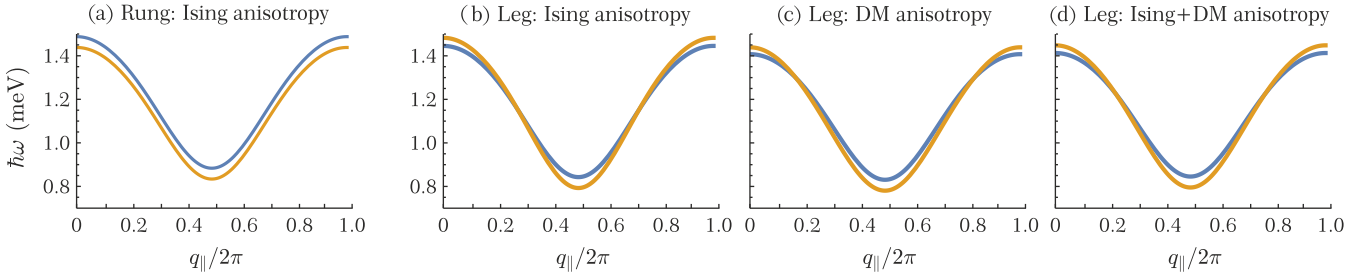
FIG. 4. Triplet dispersion for a spin ladder with exchange anisotropy: (a) Ising anisotropy on the ladder rungs, (b) Ising anisotropy on the legs, (c) DM anisotropy on the legs, and (d) both Ising and DM anisotropy on the ladder legs, in the ratio as predicted for a simple superexchange mechanism [Eq. (11)]. For these plots, isotropic $J_\perp/k_B = 12.7$ K and $J_\parallel/k_B = 3.54$ K were used, approximately describing the ladders in BPCB. Further, in all four cases the anisotropy parameter was chosen such that the triplet splitting at the band minimum amounts to 50 μeV. In all plots, the blue line shows the doubly degenerate $\epsilon_\pm(k)$ dispersion and the orange line shows the $\epsilon_0(k)$ triplet.

anisotropy to vanish. Only additional mechanisms may then lead to Ising-type anisotropy which is in principal allowed on a bond with inversion symmetry.

C. Exchange anisotropy in BPCB

For the compound BPCB with centers of inversion symmetry on the ladder rungs, we consider the following cases compatible with the crystallographic symmetry:

(a) Ising anisotropy on the ladder rungs;

(b) Ising anisotropy on the ladder legs;
(c) DM anisotropy on the ladder legs;
(d) both DM and Ising anisotropy on the ladder legs as predicted for simple superexchange [Eq. (11)].

Using the results of Sec. III, for these four cases, the triplet dispersion is plotted in Fig. 4. For these plots, we have used the Heisenberg exchange constants $J_\perp/k_B = 12.7$ K and $J_\parallel/k_B = 3.54$ K approximately describing BPCB [21]. In all cases the anisotropy parameter was chosen such that the triplet splitting at the band minimum amounts to 50 μeV.

Comparing the dispersion calculated for Ising-type exchange anisotropy on the ladder rungs [Fig. 4(a)] to the data of Fig. 2, we can clearly rule out this case as the dominant source of anisotropy in BPCB. The data qualitatively disagree with the calculated dispersion. For the case of anisotropic leg exchange, all three types of anisotropy considered give qualitatively the same dispersion [Figs. 4(b)–4(d)]. There is a doubly degenerate band with a smaller bandwidth and a nondegenerate band with larger bandwidth. In all cases the calculated anisotropy splitting is slightly larger at the band minimum than at the band maximum, just as in our data [31].

In Fig. 5 we show the triplet dispersion extracted from our data. These points were obtained from Gaussian fits to constant-$q_\parallel$ cuts, similar to the ones shown in Fig. 3. The vertical bars denote the width of the observed peaks. Fitting the calculated dispersions with anisotropic leg exchange [cases (b)–(d)] to these data, we find excellent agreement for all three cases. Indeed, the three calculated dispersions are so similar, that from our data, it is impossible to determine which type of exchange anisotropy on the ladder legs actually causes the observed band splitting in BPCB. As an example, in Fig. 5

the solid line shows the dispersion calculated for anisotropic exchange on the ladder legs given by Eq. (11) [case (d)] with fitted parameters

$$J_\perp/k_B = 12.77(1) \text{ K},$$
$$J_\parallel/k_B = 3.55(1) \text{ K}, \qquad (12)$$
$$D_\parallel/k_B = 1.44(2) \text{ K}.$$

In the parametrization of the Hamiltonian of Sec. III C, the coefficients are $\tilde{J}_\parallel = J_\parallel - D_\parallel^2/(4J_\parallel)$, $\lambda = \tilde{J}_\parallel/J_\perp$, $A = D_\parallel^2/(2J_\parallel \tilde{J}_\parallel)$, and $B = D_\parallel/\tilde{J}_\parallel$. Here, we stress that the numerical value of $D_\parallel/k_B = 1.44$ K cannot serve as an estimate for the overall magnitude of the magnetic anisotropy which should be estimated from the band splitting of 50 μeV, i.e., ≈ 0.6 K in units of kelvin.

This leaves the question of how one might experimentally determine the type of leg exchange anisotropy dominant in BPCB. The most promising route to answering this question would be to measure the triplet dispersion as a function of
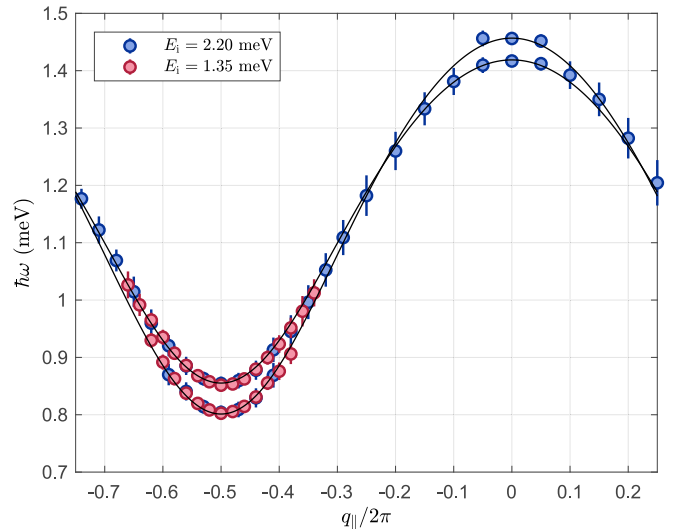

FIG. 5. Position of the triplet bands extracted from the neutron scattering data of Fig. 2. The dispersion drawn as a solid line represents a model with anisotropic interactions on the ladder legs [case (d)] as described in the text.

orientation and strength of a small applied magnetic field. In combination with calculations also including an applied magnetic field, such data might indeed allow us to determine the precise type of exchange anisotropy on the ladder legs in BPCB. However, this is clearly beyond the scope of the present work.

D. Final remarks

In BPCB the interactions on the ladder rungs are the strongest ones by far ($J_\perp \approx 3.6\,J_\parallel$). On these bonds, antisymmetric exchange anisotropy is prohibited by symmetry and only Ising-type exchange anisotropy is allowed. It may thus seem plausible to expect this to be the dominant source of anisotropy. Yet, experimentally we find that the anisotropy is predominantly due to the much weaker leg interactions of the ladder. Indeed, this is fully consistent with the theory of superexchange interactions, where symmetric and antisymmetric anisotropy contributions are always coupled. If either is prohibited by symmetry, also the other will vanish. The negligible Ising anisotropy on the ladder rungs in BPCB we thus see as supporting evidence, for the theory of anisotropic superexchange [5,6].

Since the theory of superexchange predicts DM anisotropy $B \propto |\mathbf{D}|$ and Ising anisotropy $A \propto |\mathbf{D}|^2$, initially the latter was considered subdominant [2,3]. However, both contributions are now understood to be equally important [4–6]. While not immediately intuitive, the triplet dispersions calculated in Sec. III C illustrate this effect: In the obtained expressions A appears linearly, while B only appears to second order as B^2.

Finally, we mention an apparent contradiction: Superexchange can never give rise to DM anisotropy exclusively. Yet, oftentimes pure DM interactions are used very successfully to explain anisotropy effects observed experimentally. Here, the present case study offers some illustration. For the spin ladder, different types of exchange anisotropy on the ladder legs lead to almost identical triplet dispersions that all explain our data equally well. We speculate that also in other systems one might encounter similar situations and it is for this reason that pure DM anisotropy is used so successfully to explain experimental findings, even though (within the theory of superexchange) it lacks any microscopic justification. We are only aware of one experimental study on the helimagnet $Ba_2CuGe_2O_7$, where a model employing the full Hamiltonian for anisotropic superexchange interactions [Eq. (11)] was compared to experimental data and indeed better agreement was found than for a model employing DM anisotropy only [32].

Further case studies of the nature of magnetic exchange anisotropy would certainly be interesting. We also suggest that whenever a model with pure DM interactions is considered, it would be enlightening to also consider a model with both Ising and DM anisotropy, compatible with superexchange.

V. CONCLUSION

The prototypical spin ladder compound $(C_5H_{12}N)_2CuBr_4$ (BPCB) has been studied by means of high-resolution inelastic neutron scattering. We find a small splitting of the triplet band of 50(1) μeV at the band minimum and 40(2) μeV at the band maximum. Further, for a spin ladder with exchange anisotropy, the triplet dispersion is calculated in a strong-coupling expansion.

The Ising-type anisotropy allowed by crystallographic symmetry on the ladder rungs (by far the strongest bonds) we find to be negligible, in line with the theory of anisotropic superexchange. Three models with exchange anisotropy on the ladder legs all describe the data equally well. While we cannot distinguish these by comparison to our data, we note that only one is compatible with superexchange interactions.

APPENDIX

In this Appendix we give some details on the strong-coupling expansion calculation of the triplet dispersion in a strong rung spin ladder following Ref. [27]: First, consider a single Heisenberg $S = 1/2$ spin dimer with Hamiltonian $\mathcal{H}^0 = J_\perp\,\mathbf{S}_1 \cdot \mathbf{S}_2$. The eigenstates are given by a singlet state $|s\rangle$ with energy $E_s = -\frac{3}{4}J_\perp$ and three triplet states $|t^\sigma\rangle$ with energy $E_t = \frac{1}{4}J_\perp$ and S_z spin component $\sigma = -1, 0, 1$. In all cases our calculations start from the strong rung limit, where the spin ladder is nothing but an array of L independent Heisenberg spin dimers,

$$\mathcal{H}^\perp = J_\perp \sum_{R=1}^{L} \mathbf{S}_{R,1} \cdot \mathbf{S}_{R,2}.$$

The ground state is a product of singlets $|0\rangle = |s \ldots s\rangle$ with energy $E_0 = LE_s$. The first excited states are the $3L$ degenerate single triplet states $|R, \sigma\rangle = |s \ldots t_R^\sigma \ldots s\rangle$ where the Rth rung is excited to an $S_z = \sigma$ triplet.

Now we introduce the much weaker interaction $\mathcal{H}'$ as a perturbation. It connects the individual dimers giving the spin ladder Hamiltonian $\mathcal{H} = J_\perp(\mathcal{H}^\perp + \lambda\mathcal{H}')$ with $\lambda \ll 1$. In Sec. III A, $\mathcal{H}'$ describes Heisenberg exchange connecting the dimers via the ladder legs. In addition to this, in Secs. III B and III C, $\mathcal{H}'$ also contains anisotropic exchange contributions on the ladder rungs or legs, respectively.

The ground-state energy in the presence of $\mathcal{H}'$ we denote as $\tilde{E}_0$. It is computed using standard nondegenerate Rayleigh-Schrödinger perturbation theory. The triplet states however are $3L$-fold degenerate and some care is required. The L-fold degeneracy is lifted to first order in λ and the appropriate eigenstates are Bloch waves,

$$|k, \sigma\rangle = \frac{1}{\sqrt{L}} \sum_{R=1}^{L} e^{ikR} |R, \sigma\rangle,$$

for $k = \frac{n}{2\pi}$, $n = 0, \ldots, L - 1$. In the absence of $\mathcal{H}'$ they have energy $\tilde{E}_{k,\sigma} = E_0 + J_\perp$. Further we note that all $\mathcal{H}'$ commute with $S^z = \sum_{R=1}^{L} S_R^z$ and thus with the unperturbed $\mathcal{H}^\perp$.

Therefore, they will never mix triplets with different quantum numbers σ. Starting with the $|k, \sigma\rangle$ triplet Bloch waves we can therefore again use nondegenerate perturbation theory to obtain their energy $\tilde{E}_{k,\sigma}$ in the presence of the perturbation $\mathcal{H}'$.

Calculating the ground-state energy $\tilde{E}_0$ and the triplet energy $\tilde{E}_{k,\sigma}$ to third-order perturbation theory in λ, we obtained the triplet dispersions $\epsilon_\sigma(k) = \tilde{E}_{k,\sigma} - \tilde{E}_0$. For the different $\mathcal{H}'$, these are given in Sec. III.

[1] P. W. Anderson, Phys. Rev. **115**, 2 (1959).

[2] T. Moriya, Phys. Rev. Lett. **4**, 228 (1960).

[3] T. Moriya, Phys. Rev. **120**, 91 (1960).

[4] T. A. Kaplan, Z. Phys. B: Condens. Matter **49**, 313 (1983).

[5] L. Shekhtman, O. Entin-Wohlman, and A. Aharony, Phys. Rev. Lett. **69**, 836 (1992).

[6] L. Shekhtman, A. Aharony, and O. Entin-Wohlman, Phys. Rev. B **47**, 174 (1993).

[7] M. Oshikawa and I. Affleck, Phys. Rev. Lett. **79**, 2883 (1997).

[8] I. Affleck and M. Oshikawa, Phys. Rev. B **60**, 1038 (1999).

[9] S. A. Zvyagin, A. K. Kolezhuk, J. Krzystek, and R. Feyerherm, Phys. Rev. Lett. **93**, 027201 (2004).

[10] R. Coldea, D. A. Tennant, K. Habicht, P. Smeibidl, C. Wolters, and Z. Tylczynski, Phys. Rev. Lett. **88**, 137203 (2002).

[11] M. Hälg, W. E. A. Lorenz, K. Y. Povarov, M. Månsson, Y. Skourski, and A. Zheludev, Phys. Rev. B **90**, 174413 (2014).

[12] M. Kenzelmann, A. Zheludev, S. Raymond, E. Ressouche, T. Masuda, P. Böni, K. Kakurai, I. Tsukada, K. Uchinokura, and R. Coldea, Phys. Rev. B **64**, 054422 (2001).

[13] H. Jacobsen, S. M. Gaw, A. J. Princep, E. Hamilton, S. Tóth, R. A. Ewings, M. Enderle, E. M. Hétroy Wheeler, D. Prabhakaran, and A. T. Boothroyd, Phys. Rev. B **97**, 144401 (2018).

[14] S. Bettler, F. Landolt, O. M. Aksoy, Z. Yan, S. Gvasaliya, Y. Qiu, E. Ressouche, K. Beauvois, S. Raymond, A. N. Ponomaryov, S. A. Zvyagin, and A. Zheludev, Phys. Rev. B **99**, 184437 (2019).

[15] B. R. Patyal, B. L. Scott, and R. D. Willett, Phys. Rev. B **41**, 1657 (1990).

[16] A. T. Savici, G. E. Granroth, C. L. Broholm, D. M. Pajerowski, C. M. Brown, D. R. Talham, M. W. Meisel, K. P. Schmidt, G. S. Uhrig, and S. E. Nagler, Phys. Rev. B **80**, 094411 (2009).

[17] C. Rüegg, K. Kiefer, B. Thielemann, D. F. McMorrow, V. Zapf, B. Normand, M. B. Zvonarev, P. Bouillot, C. Kollath, T. Giamarchi, S. Capponi, D. Poilblanc, D. Biner, and K. W. Krämer, Phys. Rev. Lett. **101**, 247202 (2008).

[18] M. Klanjšek, H. Mayaffre, C. Berthier, M. Horvatić, B. Chiari, O. Piovesana, P. Bouillot, C. Kollath, E. Orignac, R. Citro, and T. Giamarchi, Phys. Rev. Lett. **101**, 137207 (2008).

[19] B. Thielemann, C. Rüegg, H. M. Rønnow, A. M. Läuchli, J.-S. Caux, B. Normand, D. Biner, K. W. Krämer, H.-U. Güdel, J. Stahn, K. Habicht, K. Kiefer, M. Boehm, D. F. McMorrow, and J. Mesot, Phys. Rev. Lett. **102**, 107204 (2009).

[20] E. Čižmár, M. Ozerov, J. Wosnitza, B. Thielemann, K. W. Krämer, C. Rüegg, O. Piovesana, M. Klanjšek, M. Horvatić, C. Berthier, and S. A. Zvyagin, Phys. Rev. B **82**, 054431 (2010).

[21] D. Blosser, V. K. Bhartiya, D. J. Voneshen, and A. Zheludev, Phys. Rev. Lett. **121**, 247201 (2018).

[22] The crystal structure plots shown in Fig. 1 are based on renderings generated by the VESTA software package [33].

[23] I. Dzyaloshinsky, J. Phys. Chem. Solids **4**, 241 (1958).

[24] R. Bewley, J. Taylor, and S. Bennington, Nucl. Instrum. Methods Phys. Res., Sect. A **637**, 128 (2011).

[25] The raw data are available in the STFC Research Data Repository [34].

[26] A. Zheludev, V. O. Garlea, L.-P. Regnault, H. Manaka, A. Tsvelik, and J.-H. Chung, Phys. Rev. Lett. **100**, 157204 (2008).

[27] M. Reigrotzki, H. Tsunetsugu, and T. M. Rice, J. Phys.: Condens. Matter **6**, 9235 (1994).

[28] P. Fazekas, *Lecture Notes on Electron Correlation and Magnetism* (World Scientific, Singapore, 1999).

[29] W. Koshibae, Y. Ohta, and S. Maekawa, Phys. Rev. Lett. **71**, 467 (1993).

[30] L. Shekhtman, O. Entin-Wohlman, and A. Aharony, Phys. Rev. Lett. **71**, 468 (1993).

[31] In Fig. 4 the anisotropy parameter was chosen so as to ensure $\Delta_{\min} = 50 \,\mu$eV. For the different models of leg anisotropy (Ising only, DM only, both), this gives $\Delta_{\max} = 37, 32$ and $35 \,\mu$eV. However, since from second- to third-order perturbation expansion the dispersion still slightly changed, these small differences are probably not reliable enough to use as a criterion to select one of these three cases as the most suitable model describing the compound BPCB.

[32] A. Zheludev, S. Maslov, I. Tsukada, I. Zaliznyak, L. P. Regnault, T. Masuda, K. Uchinokura, R. Erwin, and G. Shirane, Phys. Rev. Lett. **81**, 5410 (1998).

[33] K. Momma and F. Izumi, J. Appl. Crystallogr. **44**, 1272 (2011).

[34] A. Zheludev *et al.*, Field induced $z = 2$ quantum critical dynamics in a 1d quantum magnet, STFC ISIS Neutron and Muon Sourc, doi: 10.5286/ISIS.E.87813753 (2018).